Isothermal and Nonisothermal Transition Kinetics of *trans*-1,4-Polybutadiene

Jiali Cai,[1,2] Shuqin Bo,[3] Gao Li,[3] Enle Zhou,[3] Rongshi Cheng[1]

[1]*College of Chemistry and Chemical Engineering, Nanjing University, Nanjing 210093, People's Republic of China*
[2]*Department of Biochemistry and National Laboratory of Pharmaceutical Biotechnology, Nanjing University, Nanjing 210093, People's Republic of China*
[3]*State Key Laboratory of Polymer Physics and Chemistry, Changchun Institute of Applied Chemistry, Chinese Academy of Sciences, Changchun 130022, People's Republic of China*

Received 30 January 2002; accepted 10 August 2002

ABSTRACT: Analysis of the isothermal and nonisothermal transitions of hexagonal crystal formation from the melt (transition 1) and of monoclinic crystal formation from hexagonal crystals (transition 2) for *trans*-1,4-polybutadiene (TPBD) was carefully carried out by differential scanning calorimetry (DSC) and transmission electron microscopy (TEM). Isothermal transitions 1 and 2 are described by Avrami exponents (n) of $\approx$1, whereas nonisothermal transitions 1 and 2 are described by $n \approx 4$. These different n values indicate that different crystallization mechanisms took place for different crystallization driving forces under isothermal and nonisothermal crystallization. The Ozawa equation was also used to analyze the nonisothermal crystallization data. For transition 1 at lower temperature, the Ozawa equation fits the data well; however, at higher temperature, there is an inflection that shifts to lower crystallinity with increasing temperature. Inflections are also observed with the Ozawa analysis for transition 2. Furthermore, the crystallinities at the turning points are almost in the same range as those determined by Avrami analysis for nonisothermal transitions 1 and 2, which suggests that the Ozawa analysis inflections are due to secondary crystallization. However, TEM revealed no morphology discrepancy between the TPBD hexagonal crystals formed from melt by isothermal and nonisothermal crystallization. The agreement in activation energy (ΔE) values determined by the Arrhenius and Kissinger methods indicates that the Avrami equation can describe the initial stage of transitions 1 and 2 in the nonisothermal transition process quite well. The ΔE values determined by the Arrhenius and Kissinger methods for transition 1 are 167.4 and 179.2 KJ/mol, respectively, and those for transition 2 are 186.1 and 196.3 KJ/mol; respectively. J Appl Polym Sci 89: 612–619, 2003

Key words: kinetics; activation energy; calorimetry; morphology

INTRODUCTION

trans-1,4-Polybutadiene (TPBD) is one of a considerable number of polymers that exhibit polymorphism and that exist in two crystalline forms.[1,2] One form has monoclinic packing, is stable at <76°C, and has the unit cell dimensions a = 0.863 nm, b = 0.911 nm, c = 0.483 nm, and β = 114°. The other structure exists at high temperature, is the hexagonal phase, and has the unit cell parameters a = 0.495 nm, b = 0.466 nm, and γ = 120°. TPBD has a first-order crystal–crystal phase transition; that is, the monoclinic structure transforms to the hexagonal packing above the transition temperature, and the transformation between the two forms is thermodynamically reversible.[3,4]

Recently, much attention has been paid to the study of the size-determined phase transition of TPBD.[5–9] In our previous work, detailed investigations on crystal–crystal phase transition induced by the radiation from an electron beam and the effect of size on the phase transition temperature and phase stability were carried out by differential scanning calorimetry (DSC), small-angle X-ray spectroscopy (SAXS), wide-angle X-ray diffraction (WAXD), and transmission electron microscopy (TEM).[9,10] In this paper, the isothermal and nonisothermal crystallization transition kinetics of hexagonal crystal formation from the melt and monoclinic crystal formation from hexagonal crystals was studied by DSC. The Avrami equation analysis indicates that different crystallization mechanisms took place under isothermal and nonisothermal crystallization conditions for different crystallization driving forces. This result provides a reference for improving the properties of TPBD.

Correspondence to: S. Bo (sqbo@ciac.jl.cn).

Journal of Applied Polymer Science, Vol. 89, 612–619 (2003)

EXPERIMENTAL

Materials

The samples of TPBD were synthesized with the $Al(Et)_3$-VCl_3 catalyst system, as first suggested by Natta et al.[22] Samples of TPBD were dissolved in concentrated toluene at 50°C and filtered to remove

impurities. Toluene solution was poured into a large amount of methanol to separate TPBD, and the sample was rinsed repeatedly with methanol and then placed in a vacuum oven at 50°C for 48 h. The number-average molecular weight of the sample was 8.0×10^5 as determined by analysis of the sheet formatting the powder TPBD samples and potassium bromide (KBr) was performed with a FTS135 Fourier transform IR (FTIR) spectrometer at room temperature. The FTIR spectra of the samples indicate that no *cis*-1,4 units exist. According to the formula suggested by Shen et al.,[23] the content of *trans*-1,4 units was 98.0%. Proton nuclear magnetic resonance (^{1}H NMR) experiments were performed at room temperature with a Varian Unity-400MHZ nuclear magnetic resonance apparatus after the TPBD sample was dissolved in $CDCl_3$. The content of *trans*-1,4 units was calculated as 97.5% by the ratio of the peak area of corresponding H chemical shifts of *trans*-1,4 units to the peak area of the corresponding H chemical shifts of all isomers of polybutadiene.

Sample preparation

TPBD sheets were prepared by pressing the powder samples between polytetrafluoroethylene films at 160°C and slowly cooling the sheets to room temperature for DSC experiments.

The samples for morphology observation were prepared as follows: Samples of TPBD were dissolved in 0.5% benzene, and drops of this solution were deposited on carbon-coated mica. The drops were evaporated at room temperature in a vacuum oven for 24 h. The thin films were floated off on a water surface and picked up on 400-mesh copper grids. Finally, the samples were transferred to a Perkin-Elmer DSC-7 to be isothermally and nonisothermally processed.

Differential scanning calorimetry measurements

Isothermal and nonisothermal crystallization transition kinetics were measured *in situ* with a Perkin-Elmer DSC-7 calibrated with indium and zinc standards. For isothermal crystallization, the TPBD sheet was heated to 200°C, held there for 10 min to remove all prior thermal history, and then cooled quickly to the isothermal temperature, T_c. For the nonisothermal process, the melt was first cooled from 200°C at selected constant rates, Φ (range, 2.5–60°C/min) to obtain the nonisothermal crystallization data for the hexagonal form. The sample was then reheated to 200°C, quenched to 63°C as soon as the DSC reached the temperature equilibrium, and then cooled at the same selected constant rates as already mentioned. All operations were performed under a nitrogen purge, and sample weight varied between 8 and 10 mg.

Transmission electron microscopy observation

The specimens were observed on a JEOL.JEM-2010EX electron microscope (LaB6 filament), with a side-entry goniometer and a liquid nitrogen anticontamination trap, that was operated at 200 KV. The images were recorded on photographic plates. Electron diffraction analysis was carried out with the selected-area diffraction mode on the same instrument, and calibrations for the electron diffraction patterns were occasionally made with Debye–Scherrer rings of gold evaporated on the same specimen.

RESULTS AND DISCUSSION

Isothermal crystallization kinetics analysis

Isothermal crystallization from the melt to hexagonal crystals

Provided that the relative crystallinity increases with an increase in the crystallization time t, then the Avrami equation can be used to analyze the isothermal crystallization process of TPBD, as follows:[11,12]

$$X_t = 1 - \exp[-kt^n] \tag{1a}$$

or

$$\log[-\ln(1 - X_t)] = n \log t + \log k \tag{1b}$$

where X_t is the relative volume-fraction crystallinity at time t, n is a constant whose value depends on the mechanism of nucleation and on the growth of the crystal, and k is a constant containing the nucleation and growth parameters. However, the DSC measurements only provide the relative mass-fraction crystallinity. Conventionally, the volume-fraction crystallinity, X_t, is approximated by the weight-fraction crystallinity according to the following expression:[13]

$$X_t = \frac{\int_0^t \frac{dH}{dt}\, dt}{\int_0^\infty \frac{dH}{dt}\, dt} \tag{2}$$

where dH/dt is the rate of crystallization heat evolution at time t. The double logarithmic plot of $\log[-\ln(1 - X_t)]$ versus $\log t$ is shown in Figure 1. For a crystallization temperature of 117°C, the curve in Figure 1 can be completely described by the Avrami equation with the exponent $n = 1.41$. However, for the other three temperatures (115, 114, and 112°C), each curve shows an initial linear portion that then subsequentially tends to level off, which must be described by two-stage, sequential Avrami equations. The Avrami

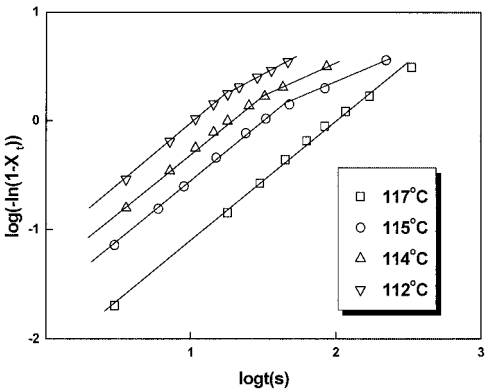

Figure 1 Double logarithmic plot of $-\ln(1 - X_t)$ versus crystallization time (t) of hexagonal crystals for isothermal crystallization at 117°C (□), 115°C (○), 114°C (△), and 112°C (▽).

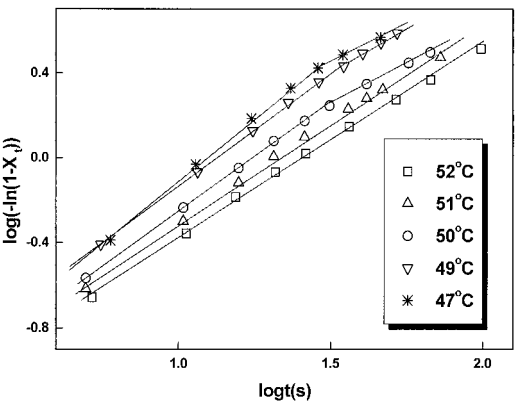

Figure 2 Double logarithmic plot of $-\ln(1 - X_t)$ versus crystallization time (t) of the monoclinic form for isothermal crystallization of the monoclinic form at 52°C (□), 51°C (△), 50°C (○), 49°C (▽), and 47°C (∗).

parameter n for the initial linear portion ranges from 0.97 to 1.20, but that for the secondary stage ranges from 0.64 to 0.71. The Avrami exponents (n) and constants (k) are summarized in Table I. Judging from the values of n, very few of the commonly accepted crystal nucleation and growth models fit the data. If one mode has to be applied, a possible crystallization mode of the hexagonal crystal of TPBD might be one-dimensional, needlike growth (for $n \approx 1$).[13] The values of the crystallization rate parameters (k) for the initial linear portion increase with an increase of supercooling.

Bermudea et al.[14] studied the kinetics of hexagonal crystallization of TPBD, with 92–96% chemical purity, by the dilatometry technique between 79.8 and 88.8°C. They observed lower crystallization rates (crystallization time up to 10,000 min), and n was shown to vary between 2.2 and 0.4 with supercooling. Grebowica et al.[15] also investigated the isothermal crystallization kinetics of the hexagonal crystal of TPBD, with almost 100% trans isomer, with a Dupont 990 thermal analyzer with a 910 DSC module between 119.8 and 104.8°C. They found that the Avrami exponent ranged from 1.26 to 0.08, which is in agreement with the data reported here if it is assumed that the first stage of crystallization was observed by Bermudez and Grebowicz et al.

Isothermal crystallization from hexagonal to monoclinic crystal

Using eq. 1, the well-known double logarithmic plots of $\log[-\ln(1 - X_t)]$ versus $\log t$ are shown in Figure 2. Similar to hexagonal crystal crystallization, the transition from hexagonal to monoclinic crystals at the higher temperatures (51 and 52°C) can be described by a one-stage Avrami equation, and that at the lower temperatures (47, 49, and 50°C) can be described by two-stage sequential Avrami equations. The Avrami exponents (n) and constants (k) are listed in Table II. The Avrami exponents (n) for the initial linear portion range between 1.22 and 0.91 and increase slightly with decreasing crystallization temperature. The Avrami exponents (n) for the secondary stage range from 0.75 to 0.8. The values of the Avrami exponents (n) for the initial linear portion are very similar to the data of Grebowicz, who obtained Avrami exponents (n) ranging between 1.74 and 0.15. However, none of the commonly accepted crystal nucleation and growth modes can describe the present data for the isothermal transition from hexagonal to monoclinic crystals.

TABLE I
Parameters k and n Obtained from Avrami Analysis of the Isothermal Crystallization of Hexagonal Crystals from Melt

T_c, °C	$n1$	$k1$	$n2$	$k2$
117	1.41	0.00568	—	—
115	1.20	0.0209	0.64	0.115
114	1.13	0.0378	0.67	0.162
112	0.97	0.0692	0.71	0.226

TABLE II
Parameters k and n Obtained from Avrami Analysis of the Isothermal Transition from Hexagonal Crystals to Monoclinic Crystals of TPBD Samples

T_c, °C	$n1$	$k1$	$n2$	$k2$
47	1.22	0.0468	0.80	0.176
49	1.06	0.0630	0.88	0.118
50	1.03	0.0527	0.75	0.133
51	0.95	0.0523	—	—
52	0.91	0.0516	—	—

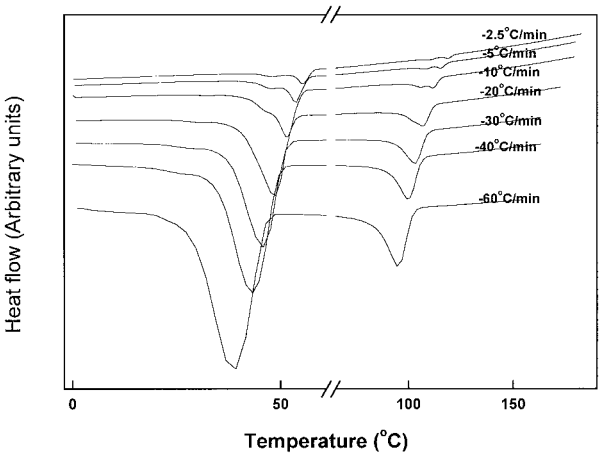

Figure 3 Heat flow versus temperature during nonisothermal melt crystallization of TPBD at the indicated cooling rates. The break in the abscissa means that the two exothermic peaks were not obtained simultaneously at sequential scanning rates. The low-temperature exothermic peaks were obtained by quenching samples to 63°C, and then scanning at the indicated scanning rates.

Nonisothermal transition kinetics analysis

Nonisothermal crystallization transition from the melt to hexagonal crystal

The cooling crystallization curves of TPBD at various cooling rates are shown in Figure 3. The exothermic peaks at higher temperature corresponds to those of nonisothermal hexagonal crystallization and the lower temperature exothermic peaks are attributed to nonisothermal monoclinic crystallization. Increasing the cooling rate results in a shift in the crystallization peak to a lower temperature. Integration of the exothermic peak during the nonisothermal scan gives the relative crystallinity as a function of temperature, which is easily transformed into a function of relative crystallinity versus time in terms of the different constant-cooling rates.[21] Considering the fact that the free spherulitic growth approximation is valid at a low degree of conversion, the initial stage of nonisothermal crystallization can be described by eqs. 1a or 1b.[16,21] The double logarithmic plots of $\log[-\ln(1 - X_t)]$ versus $\log t$ are shown in Figure 4. All the curves in Figure 4 can be described by two-stage, sequential Avrami equations. The linear portions in the first stage are almost parallel to each other, shifting to longer times with decreasing Φ. This result indicates that the nucleation mechanism was similar for the primary-stage crystallization of hexagonal crystals at all cooling rates. In the secondary stage, the straight line tends to level off at 35–58%, which suggests that the secondary-stage crystallization plays a major role in increasing the relative crystallinity of hexagonal crystal. The average value of the Avrami exponent (n) in the first stage is 4.01, which suggests that the primary crystallization stage for nonisothermal hexagonal crystallization might correspond to three-dimensional spherulitic growth with thermal nucleation.[13] The peak temperature, Avrami exponents (n), and constants (k) are summarized in Table III.

The much higher Avrami exponent ($n \approx 4$) for nonisothermal crystallization of hexagonal crystals than that ($n \approx 1$) for isothermal crystallization suggests that the mechanism for nonisothermal crystallization of hexagonal crystals is different from that of isothermal crystallization of hexagonal crystals, which may be due to the different crystallization driving forces between isothermal and nonisothermal crystallization.

TEM analysis

The different Avrami exponents (n), which indicate different crystallization mechanisms for isothermal and nonisothermal crystallization of the hexagonal crystal, prompted us to think about a possible change of end-state morphology. Therefore, TEM was used to examine morphology.

Samples on 400-mesh copper grids with carbon films were put in a Perkin Elmer-DSC-7 and processed under isothermal and nonisothermal conditions for the crystallization of hexagonal crystals. The samples from the nonisothermal crystallization process (cooled at 20°C/min) were quickly sent for TEM observation as soon as the cooled sample temperature reached room temperature. The samples formed by isothermal crystallization of hexagonal crystals at 115°C were processed for ~20 min, and then quenched to room temperature and quickly sent for observation by TEM. The end-state morphologies of the samples following the two processing conditions were the same, and

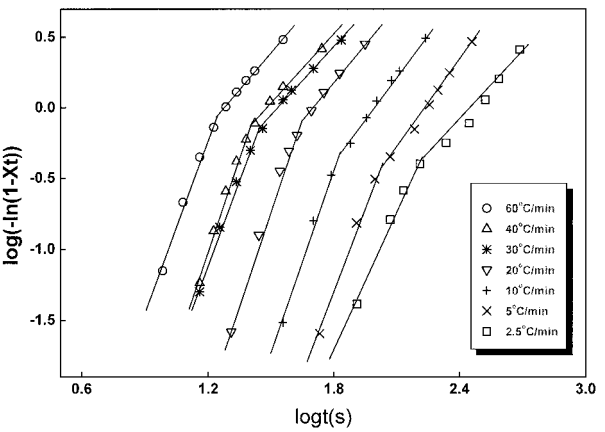

Figure 4 Double logarithmic plot of $-\ln(1 - X_t)$ versus crystallization time (t) for nonisothermal crystallization of hexagonal crystals of TPBD at different cooling rates: 60°C/min (○), 40°C/min (△), 30°C/min (∗), 20°C/min (▽), 10°C/min (+), 5°C/min (×), and 2.5°C/min (□). Lines are guides for the eye.

TABLE III
Parameters k and n Obtained from Avrami Analysis of the Nonisothermal Crystallization of Hexagonal Crystals and Nonisothermal Transition from Hexagonal Crystals to Monoclinic Crystals

	Hexagonal crystal			Monoclinic crystal		
Φ (°C/min)	T_p (°C)	$n1$	$k1$	T_p (°C)	$n1$	$k1$
60	94.8	4.18	5.99E-6	38.5	3.77	3.32E-5
40	99.8	4.87	1.38E-7	43.1	4.56	1.19E-6
30	102.9	3.84	2.01E-6	45.5	3.67	9.33E-6
20	106.8	4.47	4.03E-8	48.4	5.96	6.27E-10
10	111.6	3.98	2.26E-8	51.5	5.546	1.38E-10
5	115.4	3.798	7.64E-9	53.6	5.79	2.15E-12
2.5	118.9	3.348	1.80E-8	55.3	4.40	1.95E-10

showed no visible differences. The common characteristic morphology, shown in Figure 5, indicates that there is a spherulitic impingement between the different size spherulites, which is typical of crystallization of other normal polymers.[13] However, the lamellae of the spherulites are not well shaped. The possible difference in morphologies of the samples with different thermal histories may have been eliminated in this study by the continuing quick crystallization of the monoclinic structure when samples were cooled to room temperature.

Nonisothermal crystallization transition from hexagonal to monoclinic crystals

The cooling curves for monoclinic crystals of TPBD at various cooling rates are shown in Figure 3 together with the DSC scan of the hexagonal crystals formed under nonisothermal conditions. The exothermic peaks of monoclinic and hexagonal crystals are not simultaneously obtained at the same sequential constant cooling rate. The peak temperature shifts to lower temperature with increasing cooling rates (Table IV). The Avrami equation was also used to analyze these data: the double logarithmic plots of $\log[-\ln(1 - X_t)]$ versus $\log t$ are drawn in Figure 6. Interestingly, these plots are very similar to those obtained from the nonisothermal crystallization of hexagonal crystals; that is, each curve can be described by a two-stage sequential Avrami equation. The average value of the Avrami exponent (n) at the first stage is 4.80, which also differs from the Avrami exponent (n) for isothermal crystallization from the hexagonal to monoclinic crystals.

At the secondary stage, the straight line tends to level off in a wide range from 34 to 73% relative crystallinity. This result suggests that the secondary stage also plays a major role in increasing the relative crystallinity of monoclinic crystals during the nonisothermal process, which is analogous to the nonisothermal crystallization of hexagonal crystals. The peak temperature (T_p) and the Avrami parameters (n and k) are collected in Table III.

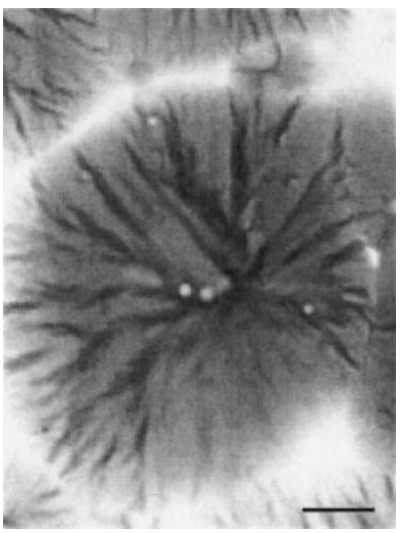

Figure 5 Characteristic TEM morphology of TPBD after isothermal and nonisothermal crystallization of hexagonal crystals (scale bar = 1 μm).

Ozawa analysis in nonisothermal crystallization kinetics

Given that the nonisothermal crystallization is a rate-dependent process, and assuming that the mathematical derivation of Evans[17] is valid, assuming the polymer melt was cooled at a constant rate, and considering the effect of cooling rate on crystallization, Ozawa modified the Avrami equation by substituting t into eqs. 1a or 1b with T/Φ as follows:[18]

$$1 - X_t = \exp[-K(T)/\Phi^m] \quad (3a)$$

or

$$\log[-\ln(1 - X_t)] = -m \log \Phi + \log KT] \quad (3b)$$

where X_t is the relative crystallinity, m is the Ozawa exponent, Φ is the cooling rate, and $K(T)$ is cooling function. The results of Ozawa's analysis for nonisothermal crystallization of hexagonal crystals, accord-

TABLE IV
Parameters Obtained from Ozawa Analysis of the Nonisothermal Crystallization of Hexagonal Crystals and Monoclinic Crystals

Hexagonal crystal			Monoclinic crystal		
T (°C)	m	Log $K(T)$	T (°C)	m	Log $K(T)$
82	0.69	1.43	41.5	2.81	4.79
83.5	0.69	1.41	43.5	3.28	4.30
85.5	0.67	1.48	46.5	3.21	4.13
89.5	0.84	1.49	48.5	3.10	3.61
95.5	1.85	2.81	49.5	3.02	3.23
99.5	2.85	4.10	—	—	—
103.5	3.40	4.41	—	—	—
105.5	3.15	3.74	—	—	—
107.5	4.14	4.77	—	—	—

ing to the double logarithmic form of eq. 3b, are presented in Figure 7, which a plot of $\log[-\ln(1 - X_t)]$ versus log Φ for temperatures ranging from 82 to 107.5°C. At lower temperatures, the Ozawa equation describes the data well. But with increasing temperatures, the $\log[-\ln(1 - X_t)]$ versus log Φ plots are no longer linear and an inflection is often observed. Furthermore, with increasing the temperature, $\log[-\ln(1 - X_t)]$ at the turning point shifts to lower values and, in fact, lower $\log[-\ln(1 - X_t)]$ means lower relative crystallinity, X_t.

The values of the relative crystallinity at the turning point are almost in the same range as those of the Avrami analysis, which suggests that the appearance of the inflection in the Ozawa analysis is attributed to the same reason; that is, the secondary crystallization.[16,19] The Ozawa exponent (m) and cooling function [$K(T)$] were obtained in the range of lower relative crystallinity (X_t) and are listed in Table IV. The Ozawa exponent (m) ranges between 4.14 and 0.67, and the cooling function [$K(T)$] increases with increasing temperature.

Similarly, the Ozawa analysis was applied to nonisothermal crystallization of monoclinic crystals, and the double logarithmic plots of $\log[-\ln(1 - X_t)]$ versus log Φ are shown in Figure 8. Similar to nonisothermal crystallization of hexagonal crystals, inflection also occurs for monoclinic crystals. Also, the values of the relative crystallinities at the turning points are almost in the same range as those from Avrami analysis for nonisothermal crystallization of monoclinic crystals; therefore, the occurrence of the inflection is also due to the secondary crystallization. The corresponding Ozawa exponents (m) and cooling functions [$K(T)$] in the lower crystallinities were also obtained and are listed in Table IV. The values of m range from 2.81 to 3.02, and $K(T)$ increases with decreasing temperature.

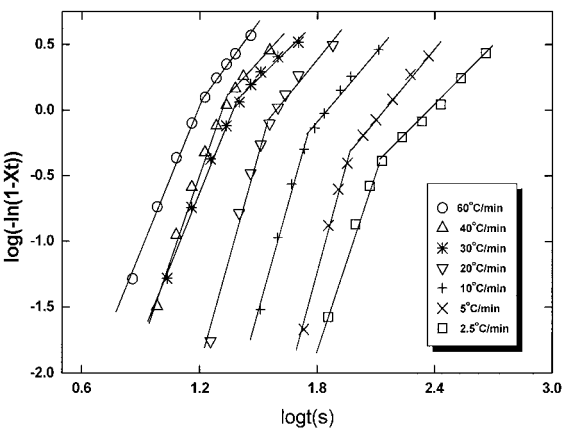

Figure 6 Double logarithmic plot of $-\ln(1 - X_t)$ versus crystallization time (t) for nonisothermal crystallization of the monoclinic form of TPBD at different cooling rates: 60°C/min (○), 40°C/min (△), 30°C/min (∗), 20°C/min (▽), 10°C/min (+), 5°C/min (×), and 2.5°C/min (□). Lines are guides for the eye.

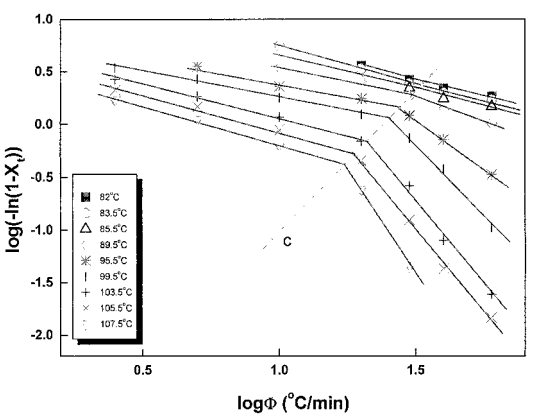

Figure 7 Ozawa plot of log $-\ln(1 - X_t)$ versus log Φ for nonisothermal crystallization of hexagonal crystals of TPBD at the indicated temperatures. Solid lines are guides for the eye, and the dashed line (c) indicates the turning points.

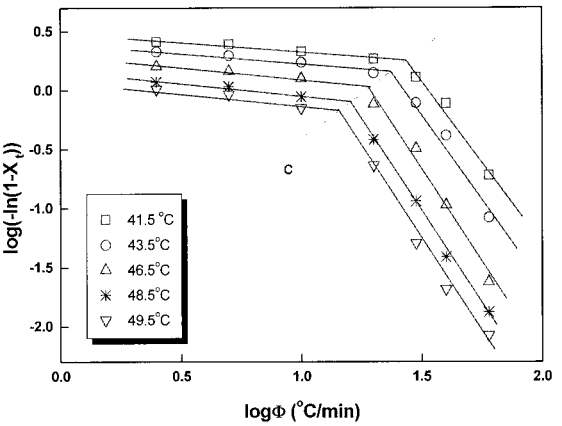

Figure 8 Ozawa plot of log $-\ln(1 - X_t)$ versus log Φ for nonisothermal crystallization of the monoclinic form of TPBD at the indicated temperatures. Solid lines are guides for the eye, and the dash line (c) indicates the turning points of Ozawa plot.

Activation energy (ΔE) of nonisothermal crystallization

If the crystallization process is assumed to be thermally activated, the crystallization activation energy can be obtained by the Arrhenius equation:[16]

$$k^{1/n} = k_0 \exp(-\Delta E/RT_c) \tag{4a}$$

or

$$(1/n)\ln k = \ln k_0 - (\Delta E/RT_c) \tag{4b}$$

where k_0 is a temperature-independent preexponential factor, R is the gas constant, T_c is the absolute temperature, and ΔE is the crystallization activation energy. A plot of $(1/n)\ln k$ versus $1/T_c$ is shown in Figure 9. The crystallization activation energy for the formation of hexagonal crystals from the melt, calculated from

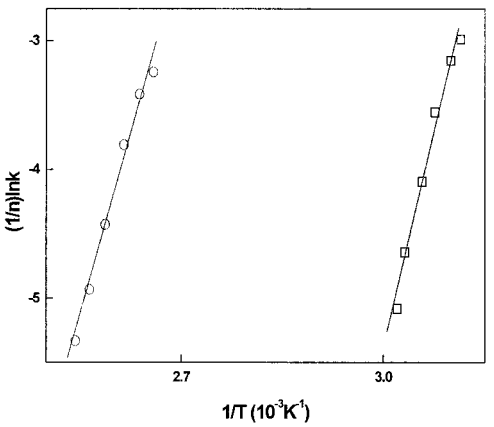

Figure 9 Plot of $(1/n)\ln k$ versus $1/T$ for Avrami parameter k and n deduced from nonisothermal crystallization data: nonisothermal crystallization of monoclinic crystal (□); nonisothermal crystallization of hexagonal crystal (○).

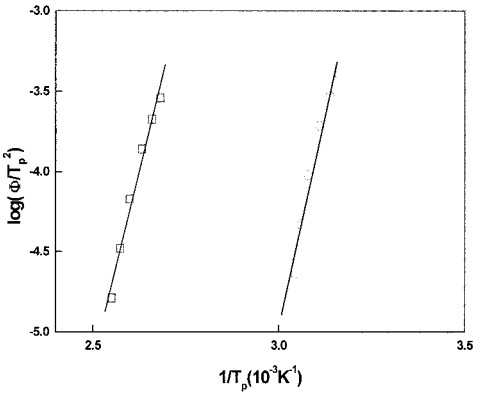

Figure 10 Kissinger plot of $\log(\Phi/T_P^2)$ versus $1/T_p$ for nonisothermal crystallization of hexagonal crystals (□) and nonisothermal crystallization of monoclinic crystals (○). Lines are guides for the eye.

the slope of the straight line; is 167.4 KJ/mol, and that for the formation of monoclinic crystals from hexagonal crystals is 186.1 KJ/mol.

In addition, accounting for the effect of cooling rate (Φ) on the peak temperature (T_p) in the nonisothermal crystallization process, the crystallization activation energy can be determined by Kissinger's method with the following equation:[20]

$$\frac{d[\ln(\Phi/T_p^2)]}{d\left(\frac{1}{T_p}\right)} = -\frac{\Delta E}{R} \tag{5}$$

where R is the cooling rate and T_p is peak temperature. Plots of $\log(\Phi/T_p^2)$ versus $1/T_p$ are shown in Figure 10. From the slopes of the curves, the activation energies are determined as 179.2 KJ/mol for hexagonal crystal crystallization from the melt and 196.3 KJ/mol for monoclinic crystal crystallization. The activation energies obtained by the Avrami and Kissinger methods are listed in Table V. The activation energies (ΔE) obtained by the two methods are in good agreement. This agreement in ΔE values determined by the Avrami and Kissinger methods suggests that the Avrami analysis does work well in describing the initial stage of nonisothermal crystallization of hexagonal and monoclinic crystals of TPBD.

TABLE V
Activation Energy of Nonisothermal Crystallization of Hexagonal Crystals and Monoclinic Crystals Obtained by the Arrhenius and Kissinger Methods

TPBD crystal forms	Activation energy (ΔE), KJ/mol	
	Kissinger method	Arrhenius method
Monoclinic	196.3	186.1
Hexagonal	179.2	167.4

CONCLUSIONS

A study of transitions of hexagonal crystal formation from the melt (transition 1) and of monoclinic crystal formation from hexagonal crystals (transition 2) of TPBD was carried out by DSC. With isothermal crystallization, whether hexagonal crystal or monoclinic crystal, the Avrami exponent (n) ranges from 1.4 to 0.64; therefore, no commonly accepted crystal nucleation and growth model can fit the data.

The Ozawa equation was used to analyze the data for the nonisothermal transition processes (transitions 1 and 2). For transition 1 at lower temperature, the Ozawa equation fits the data well. However, at higher temperature, there is an inflection that shifts to lower crystallinity with increasing temperature. For transition 2, inflections are also observed in the temperature range studied. The crystallinities at the turning points determined with the Ozawa equations analysis are almost in the same range as those determined by Avrami analysis, suggesting that the inflections are due to the secondary crystallization.

Avrami analysis of the nonisothermal transitions 1 and 2 shows that the Avrami exponent of $n \approx 4$ is different from the values obtained from the isothermal transitions. This difference indicates different crystallization mechanisms under isothermal and nonisothermal crystallization conditions. The agreement in activation energy (ΔE) values determined by the Arrhenius and Kissinger methods indicates that the Avrami equation can describe the initial stage of transitions 1 and 2 in the nonisothermal transition process. Also, the activation energies (ΔE) for transition 1, determined by the Arrhenius and Kissinger methods, are 167.4 and 179.2 KJ/mol, respectively, and those for transition 2 are 186.1 and 196.3 KJ/mol, respectively.

The authors thank the Special Funds for Major State Research Projects of China and the National Key Projects for Fundamental Research "Macromolecular Condensed State," The State Science and Technology Commission of China. The authors express their gratitude to Prof. S. Z. D. Cheng at the University of Akron for his valuable discussions. Thanks are due to Dr. W. Dong for providing TPBD sample.

References

1. Iwayanagi, S.; Sakurai, I.; Sakuri, T. J Macromol Sci Phys 1968, B2, 163.
2. Sehiro, K.; Takayanagi, M. J Macromol Sci Phys 1970, B4, 139.
3. Bermudez, S. F.; Fatou, J. G. Eur Polym 1972, 8, 575.
4. Tatsumi, T.; Fukushima, T.; Imada, K.; Takayanagi, M. J Macromol Sci Phys 1967, B1, 459.
5. Rastogi, S.; Ungar, G. Macromolecules 1992, 25, 1445.
6. Moller, M. Makromol Chem Rapid Commun 1988, 9, 107.
7. Wang, P. G.; Woodward, A. E. Macromolecules 1987, 20, 2718.
8. Finter, J.; Wegner, G. Macromol Chem 1981, 1982, 1859.
9. Yang, X. N.; Cai, J. L.; Kong, X. H.; Dong, W. M.; Li, G.; Ling, W.; Zhou, E. L. Eur Polym J 2001, 37, 763.
10. Yang, X. N.; Cai, J. L.; Kong, X. H.; Dong, W. M.; Li, G.; Zhou, E. L. Macromol Chem Phys 2001, 202, 1166.
11. Avrami, M. J Chem Phys 1939, 7, 1103.
12. Avrami, M. J Chem Phys 1940, 8, 212.
13. Wunderlich, B. Macromolecular Physics, Vol. III; Academic Press: New York, 1980.
14. Bermudez, S. F.; Fatou, J. G.; Royo, J. An Quim 1970, 66, 779.
15. Grebowicz, J.; Cheng, S. Z. D.; Wunderlich, B. J Polym Sci Part B: Polym Phys 1986, 24, 675.
16. Cebe, P.; Hong, S. D. Polymer 1986, 27, 1183.
17. Evans, U. R. Trans Farad Soc 1945, 41, 365.
18. Ozawa, T. Polymer 1971, 12, 150.
19. Liu, T. X.; Mo, Z. S.; Wang, S. Z.; Zhang, H. F. Polym Eng Sci 1997, 37, 568.
20. Kissinger, H. Z. J Res Natl Bur Stand (U.S.) 1956, 57, 217.
21. Zhu, X.; Li, Y.; Yan, D.; Fang, Y. Polymer 2001, 42, 9217.
22. Natta, G.; Porri, L.; Corradini, P.; Morero, D. Chim Ind (Milan) 1958, 40, 362.
23. Shen, Z. Q. Chin Sci 1981, 11, 1340.